

# Helium Range Viability for Online Range Probing in Mixed Carbon-Helium Beams

Jennifer Josephine Hardt<sup>a,b,c</sup>, Alexander A. Pryanichnikov<sup>d,f</sup>, Oliver Jäkel<sup>a,b,e</sup>,  
Joao Seco<sup>d,c</sup>, Niklas Wahl<sup>a,b</sup>

<sup>a</sup>Division of Medical Physics in Radiation Oncology, German Cancer Research Center – DKFZ,  
Im Neuenheimer Feld 280, 69120 Heidelberg, Germany

<sup>b</sup>Heidelberg Institute for Radiation Oncology and National Center for Radiation Research in  
Oncology, Im Neuenheimer Feld 280, 69120 Heidelberg, Germany

<sup>c</sup>Faculty of Physics and Astronomy, Heidelberg University, Heidelberg, Germany

<sup>d</sup>Division of Biomedical Physics in Radiation Oncology German Cancer Research Center –  
DKFZ, Im Neuenheimer Feld 280, 69120 Heidelberg, Germany

<sup>e</sup>Heidelberg Ion-Beam Therapy Centre, Department of Radiation Oncology Heidelberg  
University Hospital, Germany

<sup>f</sup>Institute of Biomedical Engineering (IBT), Karlsruhe Institute of Technology (KIT), Karlsruhe,  
Germany

Version 1, typeset May 5, 2025

Corresponding author(s):

Jennifer Josephine Hardt: [jennifer.hardt@dkfz-heidelberg.de](mailto:jennifer.hardt@dkfz-heidelberg.de)

## Abstract

**Background:** Recently, mixed carbon-helium beams were proposed for range verification in carbon ion therapy: Helium, with three times the range of carbon, serves as an on-line range probe, and is mixed into a therapeutic carbon beam.

**Purpose:** Treatment monitoring is of special interest for lung cancer therapy, however the helium range might not always be sufficient to exit the patient distally. Therefore mixed beam use cases of several patient sites are considered.

**Methods:** An extension to the open-source planning toolkit, **matRad**, allows for calculation and optimization of mixed beam treatment plans. The use of the mixed beam method in 15 patients with lung cancer, as well as in a prostate and liver case, for various potential beam configurations was investigated. Planning strategies to optimize the residual helium range considering the sensitive energy range of the imaging detector were developed. A strategy involves adding helium to energies whose range is sufficient. Another one is to use range shifters to increase the helium energy and thus range.

**Results:** In most patient cases, the residual helium range of at least one spot is too low. All investigated planning strategies can be used to ensure a high enough helium range while still keeping a low helium dose and a satisfactory total mixed carbon-helium beam dose. The use of range shifters allows for the detection of

more spots.

**Conclusion:** The mixed beam method shows promising results for online motioning. The use of range shifters ensures a high enough helium range and more detectable spots, allowing for a wider-spread application.

**Keywords:** carbon therapy, helium imaging, mixed beam, range verification, range shifter

---

# Introduction

Mixed beams are a recent proposition for range-guided particle therapy ( Refs. 1, 2). Hereby two ion species with the same mass-to-charge ratio, for example, fully ionized carbon ( $^{12}\text{C}^{6+}$ ) and helium ( $^4\text{He}^{2+}$ ) ions, are accelerated to the same energy per nucleon in a synchrotron-based accelerator. The experimental feasibility of creating such mixed beams was recently demonstrated: Graeff et al.<sup>3</sup> and Galonska et al.<sup>4</sup> extract a mixed beam from a single ion source using methane with helium as support gas. Kausel et al.<sup>5</sup> and Renner et al.<sup>6</sup> use a double multi-turn injection, injecting first helium and then afterwards carbon into the synchrotron ring.

With carbon and helium ions accelerated to the same energy per nucleon, the range of helium ions is about three times the range of carbon ions, as shown in figure 1. Thus, while carbon ions are the primary treatment modality, helium ions, due to their greater range, could exit the patient distally. The residual range of the helium ions could then be measured, offering the potential for an online treatment monitoring to verify the water-equivalent thickness (WET) at the irradiated spot positions. Mazzucconi et al.<sup>1</sup> and Volz et al.<sup>7</sup> discussed an additional helium fluence of 10% to ensure a low additional dose to the patient while still achieving a detectable helium signal above the carbon fragment background.

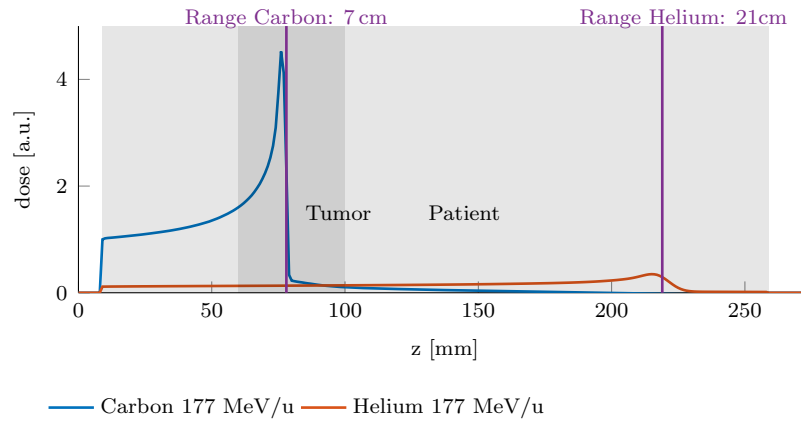


**Figure 1:** Schematic set up of a mixed carbon-helium irradiation, in this example the helium energy is not high enough for the helium ions to exit the patient distally.

Hardt et al.<sup>8</sup> demonstrated potential use cases of the mixed carbon-helium beam method in treatment verification, investigating patient positioning verification or breath hold verification. We extended the open source treatment planning tool `matRad` ( Refs. 9, 10) for mixed beam treatment planning. Including fast pencil beam dose calculation with custom high-energy helium pencil-beam kernels and exportation of the treatment plan to the Monte Carlo system, TOPAS, ( Refs. 11, 12) to allow for simulation of helium radiographs.

The pipeline for simulation of helium radiographs presented by Hardt et al.<sup>8</sup> modeled the proton radiography detector by ProtonVDA ( Ref. 13). This system was recently used for helium radiographs ( Ref. 14), as well as a feasibility study for intrafractional motion management ( Ref. 15). This system utilizes two trackers, one proximal and one distal of the patient and an energy detector distal of the patient. However with the high carbon intensities

used for radiation therapy, the proximal or front tracker is expected to be overwhelmed by the used intensity. Therefore the pipeline was extended to allow for a simulation without front tracker. The position of the ions are only measured distally of the patient. During image reconstruction the position of the ions on the front tracker is estimated from the beam monitoring system ( Refs. 16, 17). During our simulations the geometry and materials of the tracking detector is simulated, and the phase space of the primary helium ions at the position of the trackers is saved from which the images are reconstructed.

Taking a closer look at the helium range, Figure 1 shows it to be about three times the carbon range at the same energy per nucleon. However, depending on the tumor site the helium range may not be sufficient for the ions to exit the patient distally as also seen in figure 1. In lung cases, common irradiation geometries often require only a small carbon range to reach the tumor resulting in a respectively too short helium range. Complementary, for more deep seated tumors, the high residual helium range of the exiting ions can challenge the sensitive window of the detector. In this work, we investigate the expected residual helium range for several cancer sites, namely prostate, liver and lung. Next to this several helium range strategies are proposed to choose and modify the residual helium range: *EW He* (energy wise helium), *const RaShi* (constant range shifter) and *EW RaShi* (energy wise range shifter). These strategies will be presented in more detail the following section and should ensure sufficient helium range, to exit the patient distal but also consider the optimal sensitive range of the used detection system. In short, we propose irradiating only the portion of the energies in the treatment plan with sufficient helium range with a mixed carbon helium beam (*EW He*). Additionally, we propose adding proximal range shifters to increase the used helium energy, ensuring sufficient range and distal range shifters to reduce the helium range when necessary, ensuring that the residual helium energy is not too high for the detector to measure (*const RaShi*, *EW RaShi*).

During treatment planning, a raytracing algorithm ( Ref. 18) calculates the (water equivalent path length) WEPL traversed by the particle beam. This allows us to estimate the residual helium range by subtracting the traversed WEPL from the initial range.

## II Materials and Methods

### II.A Strategies to optimize the residual Helium range

#### II.A.1 Selection of energies for mixed beam irradiation

The first investigated strategy (*EW He*) to avoid mixed-in helium Bragg peaks within the patient is to limit the usage of a mixed carbon-helium beam to energies with sufficiently high helium range. This strategy would first irradiate all carbon-only energies, then switch to a mixed carbon-helium beam and irradiate the remaining energies. To implement this, the minimum residual helium range is calculated for each energy; if it is smaller than a safety margin of 10 mm, the energy is marked for irradiation with a conventional carbon beam only.

## II.A.2 Selection of proximal and distal range shifters

Since the helium range is three times the carbon range, the range of the primary carbon spot needs to be at least 1/3 of the minimum helium range required for the helium ions to distally exit the patient. To ensure that the all primary carbon spots in the target have a large enough water-equivalent range, a proximal range shifter ( $x_P$ ) can be used to adjust the proximal material budget.

Since not every helium energy can be measured by the used detection system, the use of a distal range shifters ( $x_D$ ), placed between the patient and the detector is considered. This range shifter lowers, if needed, the residual helium energy at the detection system for optimal detection properties.

We developed an algorithm to automatically choose the WET of the proximal and distal range shifter based on the residual helium range, and the sensitive range of the chosen detector. Several discrete option for the WET of the proximal ( $O_P = \{0, 5, 15, 25, 35 \text{ and } 45 \text{ mm}\}$ ), and for the distal range shifter ( $O_D = \{0, 10, 20, 30, 40, 50, 60, 70, 80, 90, 100, 110, 120, 130, 140 \text{ and } 150 \text{ mm}\}$ ) were considered. The proximal range shifter thicknesses are chosen to be consistent with range shifters already used in clinics, Wang et al.<sup>19</sup> uses range shifters with a thicknesses of up to 41.2 mm.

First we calculate which proximal range shifters ( $x_P$ ) and energy combinations ( $E$ ) are possible, i.e., if the carbon range ( $R_C(E)$ ) is within the target and if the helium range ( $R_{He}(E)$ ) is high enough for helium to traverse the entire patient. We calculate for all energy and proximal range shifter combinations the following, and only consider combinations for which this holds true

$$\mathcal{A}(x^P, E) = \begin{cases} 1, & \text{if } \text{WEPL}^{\text{TI}} \leq R_C(E) - x^P \leq \text{WEPL}^{\text{TO}} \\ & \text{and } R_{He}(E) - \text{WEPL}^{\text{PO}} - x^P \geq R^{\text{min}} \\ 0, & \text{otherwise} \end{cases} \quad (1)$$

Hereby  $\text{WEPL}^{\text{TI}}$  and  $\text{WEPL}^{\text{TO}}$  are the traversed WEPL at the tumor entrance and exit and  $\text{WEPL}^{\text{PO}}$  the total WEPL of the patient. The safety margin of the minimum allowed residual helium range ( $R^{\text{min}}$ ) distal of the patient is 10 mm.

For each of the available combinations we then estimate if the helium ions will be detectable by our chosen detector, i.e if the residual helium range is in the sensitive range of the detector denoted as  $[R^{\text{minD}}, R^{\text{maxD}}]$ . For this we calculate:

$$\mathcal{D}(x^P, x^D, E) = \begin{cases} 1, & \text{if } R^{\text{minD}} \leq R_{He}(E) - \text{WEPL}^{\text{D}} - x^P - x^D \leq R^{\text{maxD}} \\ 0, & \text{otherwise} \end{cases} \quad (2)$$

Whereby  $\text{WEPL}^{\text{D}}$  is the traversed WEPL at the entrance of the detector. Contrary to  $\text{WEPL}^{\text{PO}}$  this could include the WEPL of patient couch.

During investigation the minimal detectable range was set to  $R^{\min D} = 7.5$  mm, for the maximum detectable range two imaging detectors, were investigated one with a smaller ( $R^{\max D} = 110$  mm), and one with a larger sensitive range ( $R^{\max D} = 160$  mm).

Two approaches were considered for selecting the optimal range shifter. In the first method, each treatment field has a single fixed proximal and distal range shifter for all delivered energies (*const RaShi*). In contrast, the second method allows energy-dependent selection of the proximal range shifter (*EW RaShi*). The concept behind this approach is that the proximal range shifter could be attached to the nozzle, enabling a quick selection of a different thicknesses for a different energy. However, the distal range shifter thickness remains unchanged throughout the delivery of the treatment field.

**Const RaShi** To determine the optimal combination of proximal and distal range shifters for a field, we strive for a high detection percentage while minimizing the WET thickness of the selected range shifters. A greater thickness leads to increased beam broadening and image noise. Therefore, we maximize the weighted sum of of the number of detectable spots and the total thickness of the applied range shifters:

$$[x^{P*}, x^{D*}] = \operatorname{argmax}_{\substack{x^P \in O^P \\ x^D \in O^D}} \left( \frac{1}{n_1} \left( \sum_{s \in \mathcal{F}} \mathcal{D}(x^P, x^D, E_s) \right) - \frac{w}{n_2} (x^P + x^D) \right). \quad (3)$$

The sum is performed for all spots  $s$  belonging to the treatment field  $\mathcal{F}$ . The parameter  $w$  serves as a relative weighting factor, of the number of detectable spots to the thickness of the range shifters. The factors  $n_1$  and  $n_2$  normalize both parts of the function to have equal magnitude

$$n_1 = \max_{\substack{x^P \in O^P \\ x^D \in O^D}} \left( \sum_{s \in \mathcal{F}} \mathcal{D}(x^P, x^D, E_s) \right) \quad (4)$$

$$n_2 = \max_{\substack{x^P \in O^P \\ x^D \in O^D}} (x^P + x^D) \quad (5)$$

**EW RaShi** Selecting the optimal proximal range shifter, while allowing for varying thicknesses across different energies, is more complex, since a given depth in the patient can be reached through multiple energy and proximal range shifter combinations. Therefore we group the spots into intervals ( $I_i$ ) of approximately the same carbon Bragg peak position in the patient ( $R_C^P = R_C - x^P$ ). The width of each interval is the chosen longitudinal spot spacing  $l$ . With this interval  $I_i$  is given as

$$I_i = [\min(R_C^P) + il, \min(R_C^P) + (i + 1)l] \quad i = 0, 1, \dots, N. \quad (6)$$

Whereby the last interval  $I_N$  includes the most distal carbon range position ( $\max(R_C^P)$ ).

For each distal range shifter ( $x^D$ ) and carbon range interval ( $I_i$ ), the optimal proximal range shifter ( $x_{iD}^{P\star}$ ) with corresponding energy ( $E_{iD}^\star$ ) combination is selected, as the one yielding the highest number of detectable spots.

$$[x_{iD}^{P\star}, E_{iD}^\star] = \operatorname{argmax}_{x^P \in O^P} \left( \sum_{s \in I_i} \mathcal{D}(x_s^P, x^D, E_s) \right). \quad (7)$$

The number of detectable spots for this range interval ( $I_i$ ) with optimized settings, is  $\mathcal{D}_{iD}$ . The optimal proximal range shifters with their corresponding beam energy is chosen for each distal range shifter option. To determine which distal range shifter ( $x^{D\star}$ ) with corresponding proximal range shifters should be used, the total number of detectable spots is maximized while minimizing the overall thickness of the selected range shifters, similar to the *const RaShi* selection.

$$x^{D\star} = \operatorname{argmax}_{x^D \in O^D} \left( \frac{1}{n_1} \left( \sum_{i=0}^N \mathcal{D}_{iD} \right) - \frac{w}{n_2} \left( \sum_{i=0}^N x_{iD}^{P\star} + x^D \right) \right) \quad (8)$$

Whereby the normalization is given as

$$n_1 = \max_{x^D \in O^D} \left( \sum_{i=0}^N \mathcal{D}_{iD} \right) \quad (9)$$

$$n_2 = \max_{x^D \in O^D} \left( \sum_{i=0}^N x_{iD}^{P\star} + x^D \right) \quad (10)$$

### II.A.3 Incorporating proximal range shifters in dose calculation

To model the additional beam broadening caused by range shifters, Monte Carlo simulations were conducted using TOPAS version 3.9. The simulations employed the following physics list: G4DecayPhysics, G4StoppingPhysics, G4EmExtraPhysics, G4EMStandardPhysics\_option4, G4HadronElasticPhysics, g4h-phy\_QGSP\_BIC\_HP and G4QMDReaction physics. To accurately model helium ions G4BinaryLightIonReaction was activated with the Tripathi cross section data ( Ref. 20) as modified by Horst et al.<sup>21</sup>.

The simulations included carbon and helium beams at five different energies within the carbon treatment energy range (88.83, 196.23, 272.77, 339.80 and 427.44 MeV/u). Energy deposition was scored in a cylindrical volume, with a range shifter placed in front of it. Seven different water equivalent thicknesses of the range shifter were used ( $x^P = 5, 10, 15, 20, 25, 30, 35, 40$  and  $45$  mm). The range shifter was positioned at the nozzle and thus separated from the cylinder's surface at the isocenter by approximately 1 m of air.

The lateral entrance dose was fitted with a Gaussian function, and the initial beam width was subtracted quadratically to estimate the beam broadening induced by the range shifter ( $\sigma_{RaShi}$ ). A polynomial function was then fitted to interpolate beam broadening at

intermediate energies. During dose calculation, the estimated beam broadening from the range shifter is added to the initial beam width ( Refs. 9, 22).

## II.B Investigated patient cases

We analyzed the residual helium range in 15 lung cancer patient cases ( Ref. 23), considering five different gantry angles:  $0^\circ$  and  $180^\circ$ , as well as  $45^\circ$ ,  $90^\circ$  and  $135^\circ$  for tumors in the right lung or  $315^\circ$ ,  $270^\circ$  and  $225^\circ$  for tumors in the left lung. An example patient is shown in figure 2.

Additionally, we conducted a detailed analysis of one patient (No. 114) by generating treatment plans for a gantry angle of  $270^\circ$  across all residual helium range strategies. The dose influence matrix was calculated using a regular spot grid with lateral spacing of 5 mm and a longitudinal spacing of approximately 2 mm (depending on available energies) on a  $3\text{ mm}^3$  dose grid. The RBE-weighted carbon ion dose (LEM I) was optimized to 2.3 Gy per fraction for the target PTV.

Furthermore, we examined the residual range in a prostate cancer patient ( Ref. 24), with both a low-dose PTV (56 Gy) and a high-dose PTV (68 Gy), evaluating gantry angles of  $45^\circ$ ,  $90^\circ$ ,  $270^\circ$  and  $315^\circ$ . For a liver cancer patient ( Ref. 24), we investigated gantry angles of  $0^\circ$ ,  $315^\circ$  and  $270^\circ$ .

For the prostate and liver cases, we assigned a relative weighting factor  $w$  of 0.25 (equation 3), prioritizing more the number of detectable spots. For the lung cases, this weighting factor was set to 0.5. An overview of the investigated tumor sites and corresponding gantry angles is provided in figure 2.

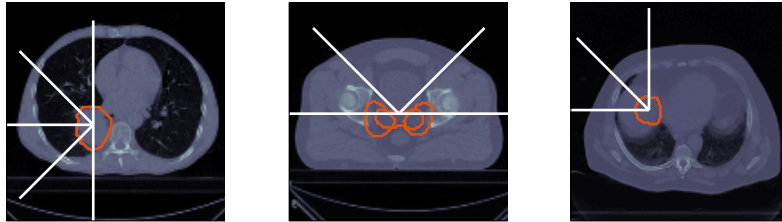


**Figure 2:** Left: Example lung patient from the lung data set, outlined is the target volume (—) and the gantry angles for which the residual helium range was investigated. Middle: Prostate case, Right: Liver case

## III Results

### III.A Residual Range analysis for different cancer sites

#### III.A.1 Lung cases

During the investigation of the residual helium range, none of the previously mentioned helium range strategies were applied; instead, conventional treatment plans were created, as the first phase of this study aimed to evaluate the necessity of such strategies. Figure 3 provides an overview of the minimum residual helium range for each investigated gantry



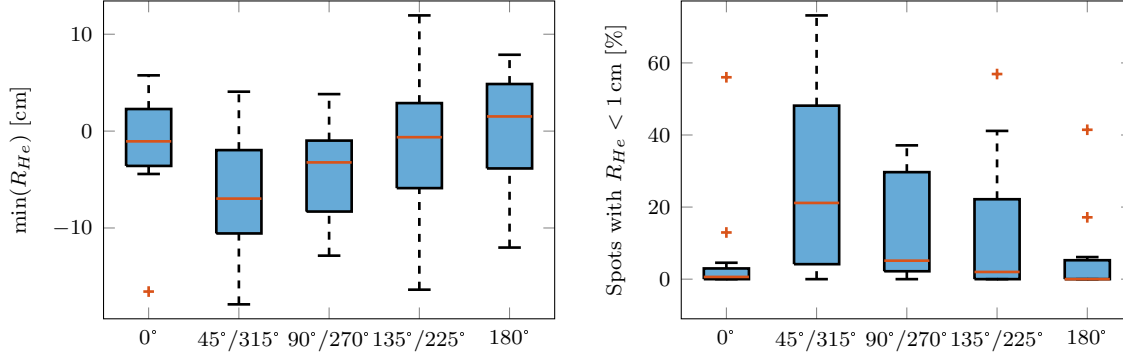


**Figure 3:** Left: Box plot summarizing the minimum residual helium range of each lung patient for the different gantry angles. Right: Box plot summarizing the percentage of spots in each treatment plan with a residual helium range smaller than 1 cm for each gantry angle.

angle and patient case, along with the percentage of spots where the residual helium range is less than 1 cm. This serves as an indication of the severity, helping to determine whether only a small or large fraction of spots are identified as having insufficient range. Negative values indicate spots where the helium ions lacked sufficient energy to exit the patient distally.

Among the examined angles, 0° and 180° appear to be the most suitable, for mixed beam irradiation without range shifters, as they offer a higher minimum residual helium range and a lower percentage of spots with insufficient range. However, 0° may be preferable to 180° since it avoids irradiation through the patient couch. Despite this, for 9 out of the 15 patients analyzed, the minimum residual helium range for a gantry angle of 0° was still below the 1 cm safety margin. Furthermore, in 6 of the 15 cases, none of the investigated angles provided sufficient range. The most frequently available angle was 180° (8/15) followed by 0° and 135/225° (6/15).

Figure 4 uses an exemplary lung patient (No. 114) to illustrate the distribution of spots with sufficient and not sufficient helium range. For the 315° gantry angle, it is particularly evident that the helium beam is most affected in regions where it must pass through the spine.

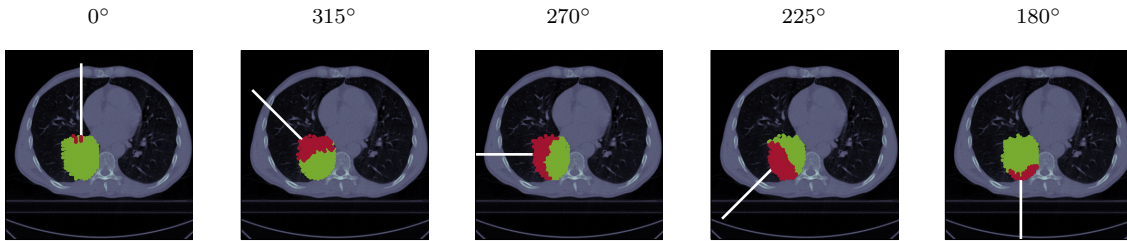


**Figure 4:** Axial CT slice for patient No.114 for different gantry angles. The overlay highlights the spots with sufficiently large residual helium range in green (●) and the ones with insufficient residual helium range in red (●).

### III.A.2 Prostate Case

In the prostate case, the residual helium range was examined for four gantry angles. Compared to the lung case, much fewer spots were affected by insufficient residual helium

range. Specifically, only 1.1 % of spots exhibited insufficient helium range for the 90° angle, which represented the highest percentage of spots with insufficient helium range among the four investigated angles. For the other angles, the percentages were 0.9 % ( 270°), 0.2 % ( 45°), 0 % ( 315°). Despite the prostate being centrally located within the patient, which might suggest that residual helium range would not be a concern, it still is.

### III.A.3 Liver Case

For the liver case, the residual helium range was analyzed for three gantry angles. All three angles exhibited spots with insufficient residual helium range. For the 0° gantry angle, only 1 % of the spots were flagged as insufficient, whereas 47 % and 38 % of spots were flagged as insufficient in the 270° and 315° angles, respectively.

## III.B Beam broadening due to range shifters

Figure 5 shows the estimated beam widening  $\sigma_{RaShi}$  caused by the use of proximal range shifter as well as the interpolated function. Especially for low energy's and a thick range shifter the broadening is large. However, this combination is infrequently used in treatment plans. Normally a thicker range shifter will be used with a higher helium energy. Not for all carbon energy's and proximal range shifter combinations the widening was calculated, for the lowest energy the used range shifter were sometimes thicker than the corresponding carbon range. This would also mean that these energies would not be used in a treatment plan, and thus it is nor necessary to calculate the helium widening in these cases, however this was done for completeness. This beam broadening was used in the following dose calculations.

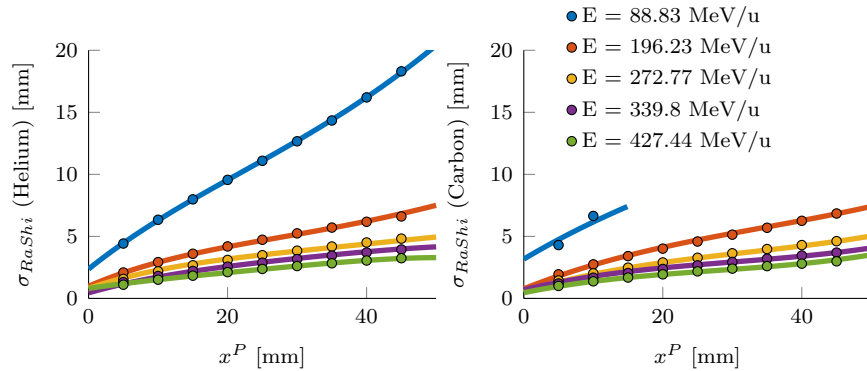


**Figure 5:** Estimated (●) and fitted (—) Beam widening due to the use of a proximal range shifter of varying thicknesses for helium (left) and carbon (right).

## III.C Strategies to optimize the residual helium range

In general, all residual helium range strategies effectively ensure a sufficient helium range. The strategies are compared based on the percentage of detectable spots. Helium ions may not be detectable for two main reasons: they are lost in the distal range shifter or their residual energy is too high for the detector to measure.

### III.C.1 Lung cases

Figure 6 presents the percentage of detectable spots across all treatment angles and patients for the presented residual helium range strategies. The calculation was conducted for two imaging detectors, one with a smaller and one with a larger sensitive range. As a reference, a treatment plan was calculated without applying any residual helium range strategy, meaning that this plan may include spots with an insufficient helium range. As expected, the larger detector with wider acceptable residual helium range allows for a larger percentage of detectable spots. Still, the difference between the two detectors is relatively small for the best-performing method, *EW RaShi* and averages 5 pp. Among the strategies, *EW He* performs the worst, even falling below the reference plan. When comparing the two range shifter strategies, the added flexibility of the *EW RaShi* method results in an average increase in detectable spots of 12 pp for the detector with the smaller sensitive range and 4 pp for the larger one. However, for the detector with the larger sensitive range, smaller distal range shifters are used on average, which would enhance image quality.

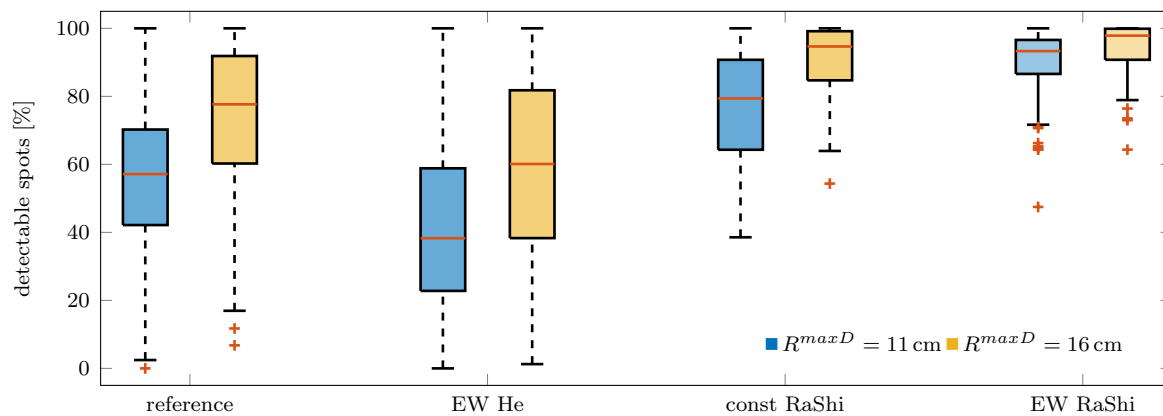


**Figure 6:** Box plot summarizing the percentage of detectable spots in the lung treatment plans for a detector with a sensitive range up to 11 cm and a bigger detector with a sensitive range up to 16 cm.

### III.C.2 Lung case No.114

To look at the different strategies in more detail, the delivered dose was optimized and calculated for an example patient. Table 1 lists the percentage of detectable helium spots, and since the optimal fluence of each spot was now calculated, the percentage of detectable helium ions was also calculated. When calculating the percentage of detectable helium ions for the *EW He* method, not the total amount of delivered helium ions was used, but 10% which is the carbon-helium ratio, of the carbon ions used. This allows a better comparison between all strategies. For the reference and *EW He* strategies, the percentage of detectable helium ions increases while the percentage of detectable ions decreases for the *const RaShi* strategy, when compared to the percentage of detectable spots. Due to higher fluence of the intermediate energies, which are detectable by the reference plan, the reference and *const RaShi* have the same percentage of detectable helium ions, although the percentage

	reference	<i>EW He</i>	<i>const RaShi</i>	<i>EW RaShi</i>
detectable spots [%]	55	35	76	93
detectable Helium ions [%]	69	46	70	93

**Table 1:** Percentage of detectable spots and helium ions for each method

of detectable spots is significantly higher for the *const RaShi* strategy. A range shifter of only 1.5 cm (*const RaShi*) already allows the detection of 24 pp more helium ions than with the *EW He* method and as many helium ions as with the reference plan, but with sufficient residual helium range.

Figure 7 provides a closer look at the selected proximal range shifter thickness, which treatment energies used helium, and the last row shows the residual helium range at the detector versus the carbon range in the patient, overlaid with the used proximal range shifter thickness. No distal range shifters were used in this case and the smaller detector ( $R^{maxD} = 11$  cm) was used. The *EW RaShi* strategy uses thicker proximal range shifters than the *const RaShi* strategy. Looking at the lower right plot, it is clear that the thickest proximal range shifter is used for the lowest carbon range in the patient and the lowest energy, and then the thickness of the proximal range shifter decreases. Note how the proximal range shifter is used to "push back" the residual helium range into the sensitive range of the imaging detector. So while the *EW RaShi* method has 23 pp more detectable helium ions than the *const RaShi*, it comes at the cost of a thicker proximal range shifter. For the *EW He* strategy, helium is used only with high energies, where the helium range is sufficient. Also noteworthy for the *const RaShi* method is that the smallest carbon range is not irradiated. These spots must have too low helium range and were therefore excluded, but a thicker range shifter would have come at the cost of a reduced number of detectable spots.

The mixed carbon-helium and helium doses for all strategies are shown in figure 8 with the respective difference from the reference plan. Figure 9 shows the corresponding carbon-helium and helium dose-volume-histograms. The residual helium range strategies reduce the delivered helium dose. This is particularly noticeable for the *EW He* method with a significant reduction in helium dose to the PTV, left lung, heart and body. However, since the helium dose contributes little to the total dose, the dose reduction is barely visible in the mixed-dose DVH.

Strategies involving range shifters introduce increased lateral scatter as visible in figure 8 as a widened dose profile and resulting increase in dose to the right lung. The mean dose increases from 0.28 Gy (reference) to 0.31 Gy (*const RaShi*) and 0.33 Gy (*EW RaShi*). For these plans, there is also a reduction in target coverage: the  $D_{95}$  value of the PTV decreases from 2.19 Gy (Reference) to 2.13 Gy (*const RaShi*) and 2.16 Gy (*EW RaShi*). In general, using range shifters increases the total delivered dose of the plans over the reference plan, in this case 10 % (*const RaShi*) and 13 % (*EW RaShi*). For all plans, the contribution of helium to the total RBE-weighted dose is less than 1 %, being 0.57 % (reference), 0.26 % (*EW He*), 0.50 % (*const RaShi*) and 0.48 % (*EW RaShi*).

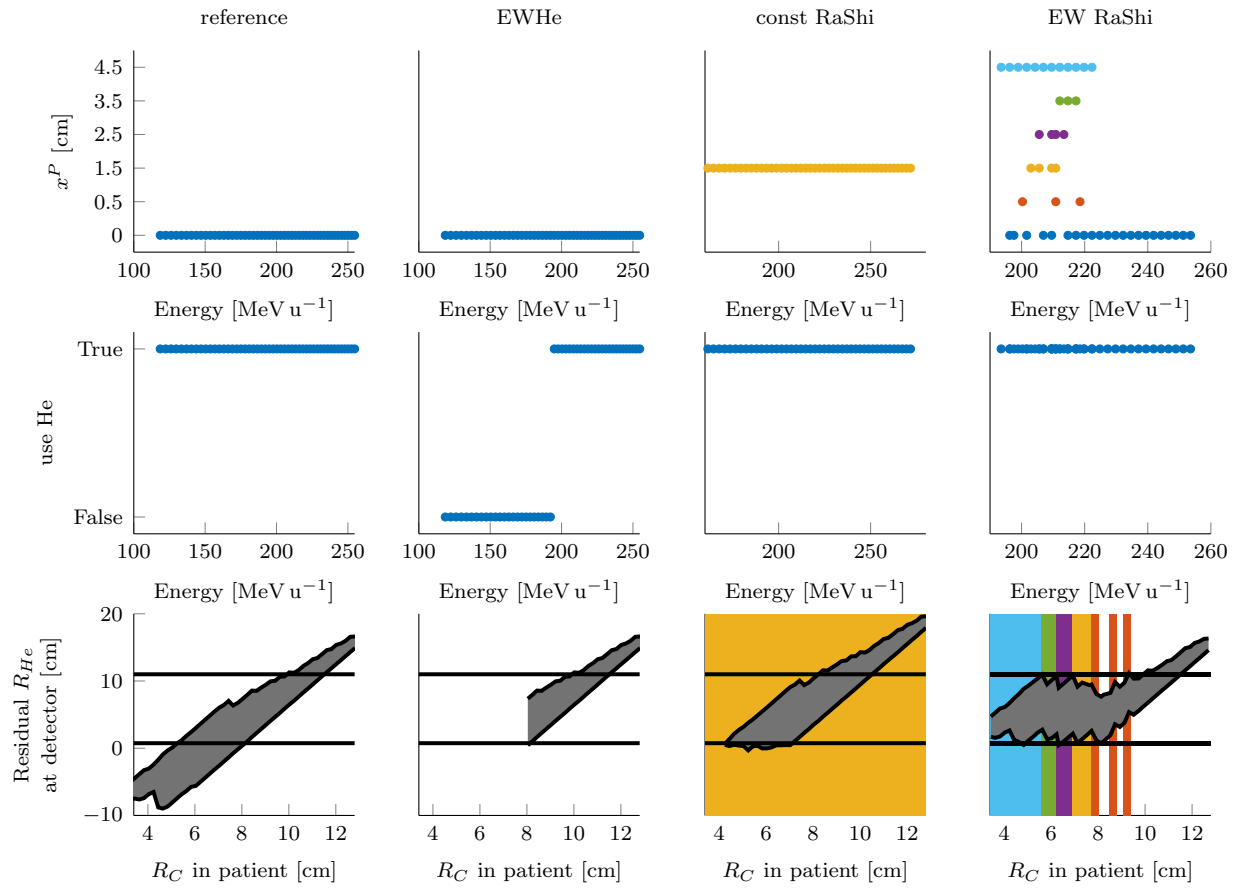


**Figure 7:** For each strategy (by column) the top row shows the proximal range shifter thickness per energy in the treatment plan. In the middle row illustrates the decision of mixing helium (True) into the carbon beam or not (False) for each energy. The bottom row displays the residual helium range at the detector for each carbon spot position in the patient. Highlighted is the minimum (0.75 cm) and maximum (11 cm) detectable range and the used proximal range shifter thicknesses. Whereby ■ represents a proximal range shifter thickness of 45 mm, ■ 35 mm, ■ 25 mm, ■ 15 mm and ■ 5 mm

### III.C.3 Prostate case

The prostate case exhibits large residual helium ranges for some energy layers and gantry angles, with the residual range reaching up to 45 cm at a gantry angle of 90°. These large residual helium ranges complicate the detection. The *EW RaShi* method has the highest percentage of detectable spots. Still for opposing beams (90°, 270°) it is only 56 % for the detector with the smaller sensitive range. For the detector with the bigger sensitive range, it increases to 69 %. The other two investigated angles (45°, 325°) have a higher percentage of detectable spots. For the smaller detection system 72 % can be detected, for the larger system this increases to 89 %. In the prostate case the residual helium range strategies selected distal range shifters.

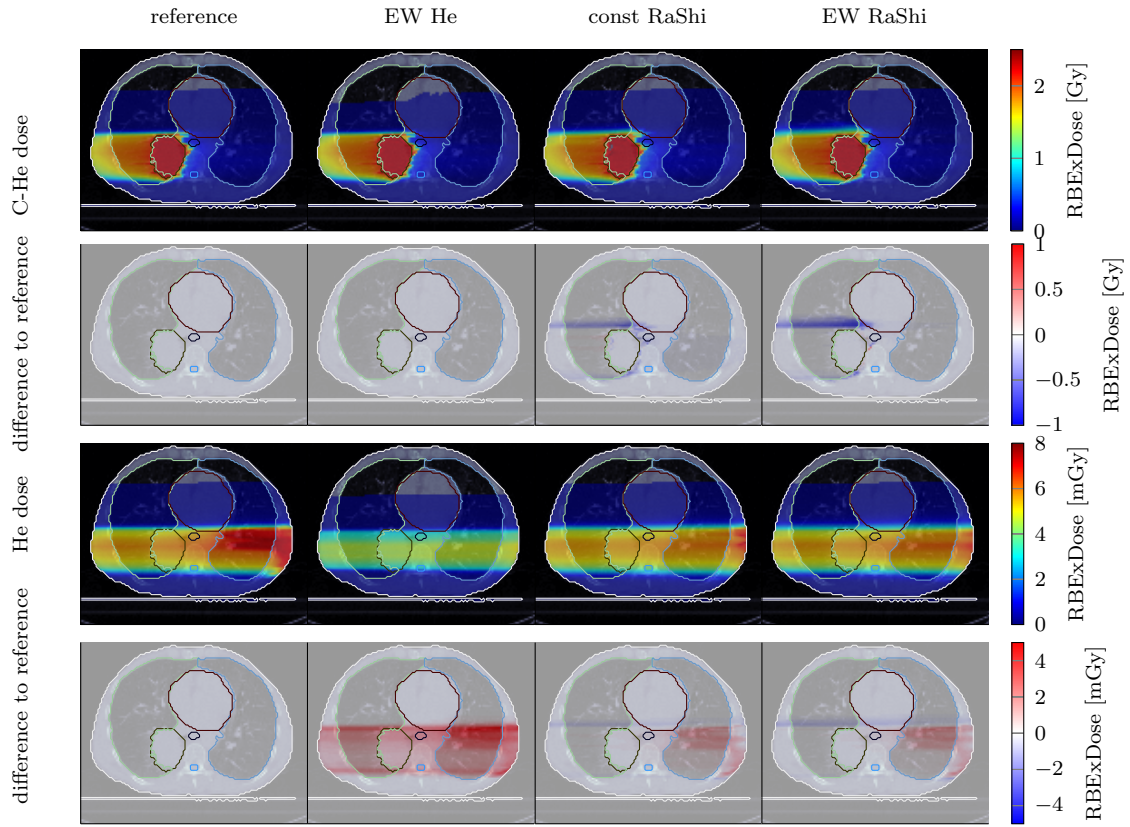


**Figure 8:** Axial dose slices for each strategy. Top: total mixed carbon-helium RBE weighted doses and below the difference to the reference plan. Bottom: Helium RBE weighted dose and the difference to the reference plan, please note the mGy scale in this case.

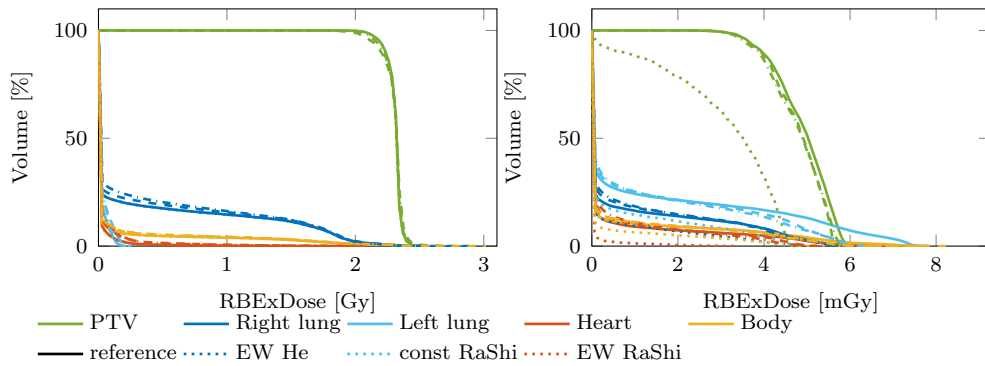


**Figure 9:** Dose-volume histogram for the different strategy's. The left DVH shows the total mixed carbon-helium RBE weighted dose, while the right DVH singles out the helium dose (on a mGy scale).

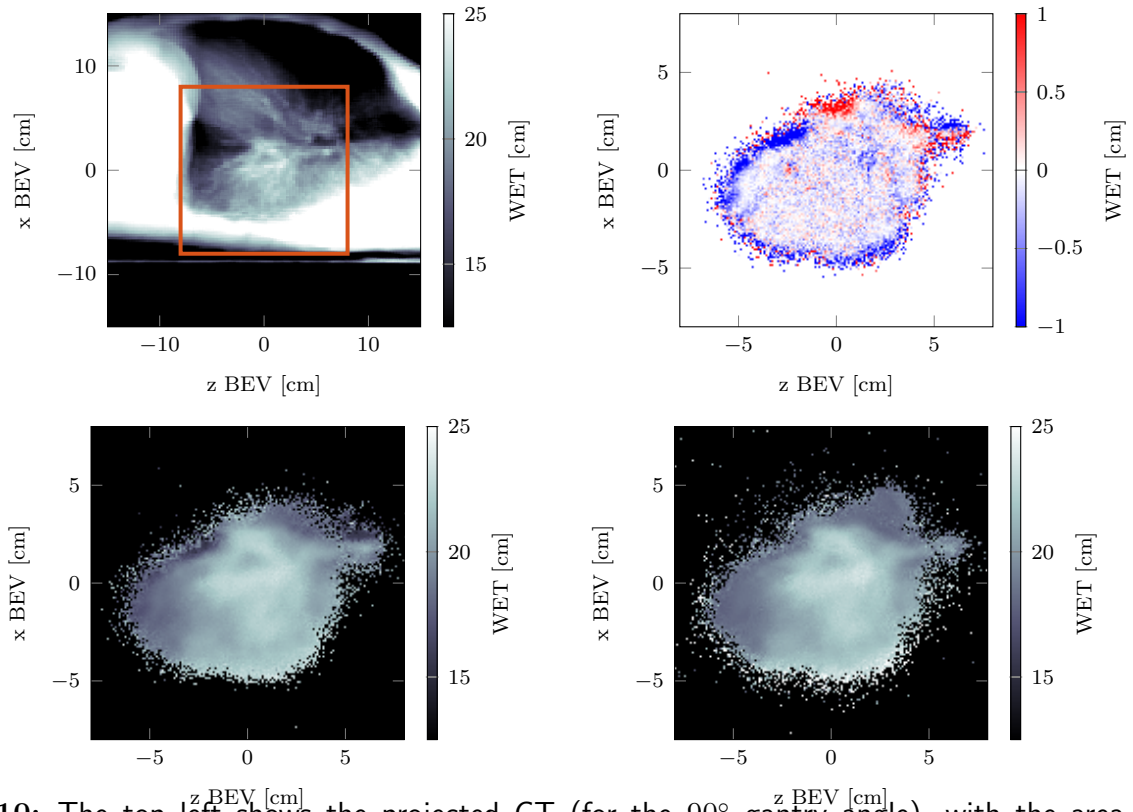


**Figure 10:** The top left shows the projected CT (for the  $90^\circ$  gantry angle), with the area highlighted (—) chosen for the mixed-beam radiographs in the other subfigures. Bottom left: Simulated helium radiograph ( $197.58 \text{ MeV u}^{-1}$ ,  $0 \text{ cm}$ ). Bottom right: Simulated helium radiograph ( $217.25 \text{ MeV u}^{-1}$ ,  $1.5 \text{ cm}$ ). Top right: Difference Image of both radiographs

### III.C.4 Liver case

For the liver case, the *EW RaShi* continued to show the highest percentage of detectable spots; up to 89 % were detectable for a gantry angle of  $270^\circ$  using the detector with reduced range sensitivity. Using the detector with the bigger sensitive range enabled detection of 97 % of the spots. Only for one gantry angle,  $0^\circ$ , a distal range shifter was used.

## III.D Helium radiographs with range shifter

In figure 10 two helium radiographs are compared, one acquired from the reference plan and the other acquired from a *const RaShi* plan. The energies of the helium radiographs were chosen so that both plans with and without range shifter, irradiate approximately the same cross-section of the tumor. The difference of both radiographs also indicates an increase in image noise when adding range shifters.



## IV Discussion

This study used a mixed carbon-helium beam treatment planning framework to investigate the applicability and limits of the mixed beam method imposed by residual helium ranges at different patient sites, with a focus on lung patients. Residual helium range is a limiting factor in the selection of patients and treatment angles, as not all combinations are sensible without mitigating strategies. Two key considerations were identified: first, the helium ions must have sufficient range to exit the patient distally; second, the residual range should be in the sensitive range of the detector, as if the range is too high, the helium ions cannot be detected.

The analysis of the helium range, without any applied helium range strategy, showed insufficient helium range for at least one energy layer in almost all cases, independent of the gantry angle. The sensitive range of the employed detector was found to be a critical factor in ensuring good detection properties. This is particularly relevant for the prostate case, where the helium ions had a greater residual helium range, requiring a larger sensitive range of 16 cm or more. For the lung sites with, in general, a smaller residual helium range, it seems that the smaller detector ( $R^{maxD} = 11$  cm) is sufficient to enable good detection properties, when a residual helium range strategy such as the *EW RaShi* is used. Under this approach, the mean increase of detectable spots, between both investigated detectors was only 5 pp. However, the maximum increase of detectable spots was 26 pp. Therefore, depending on the patient site and gantry angle, a detector with a larger sensitive range might still be sensible. An argument for a detector with a larger sensitive range is also that thinner distal range shifters were used with this detector, increasing image quality.

The detectors used by Mazzucconi et al.<sup>1</sup> and Volz et al.<sup>7</sup> for the experimental exploration of the mixed beam method covered a total WET of  $\sim 127$  mm and  $\sim 180$  mm. While most detectors currently used in ion imaging are calorimeters or range telescopes, measuring residual energy or range, other detection systems are also used. Gehrke et al.<sup>25</sup> uses a thin silicon pixel detector for helium radiography, which measures deposited energy. However, this system has a very sensitive WET range, as the most accurate WET measurement is achieved in the steep gradient of the Bragg peak. Therefore, for accurate imaging of complex objects, multiple energies are used ( Ref. 26). Another approach measures the time-of-flight (TOF) of an ion between two or more tracking units, from which the velocity and kinetic energy can be calculated. The sensitive WET range of such a detector depends on the distance between the tracking units and their time resolution ( Refs. 27, 28). A detector designed for mixed beam radiotherapy should be capable of handling high particle fluxes, offer a large sensitive range, and provide particle identification to distinguish helium signals from those of fragments.

For the lung cases, gantry angles of  $0^\circ$  and  $180^\circ$  appear most suited for radiation therapy, as only a small portion of the spots exhibit insufficient residual helium range. These angles could also be combined in a two-field treatment plan, where the upper region of the tumor is treated with a  $180^\circ$  gantry angle, while the lower region is irradiated with a  $0^\circ$  gantry angle, treating only spots with sufficient helium range from each angle. In the prostate case, a similar strategy could be used with opposing gantry angles of  $90^\circ$  and  $270^\circ$ . However, the



limitation of this strategy is that only very few centers use carbon gantries like, e.g., the HIT (Heidelberg Ion Therapy Center). Most facilities use fixed beam lines instead and are limited to horizontal and vertical orientations, with a few offering an oblique beam line \*. A fixed beam line may offer an advantage over a gantry for mixed beam irradiation, as it could simplify the setup of a distal range shifter. For more flexibility with treatment angles in the mixed beam irradiation, upright particle therapy ( Ref. 29) would be beneficial.

A disadvantage of using range shifters to optimize the residual helium range is that they introduce additional scattering, leading to beam broadening and an increased dose delivered to the patient. In addition to increased scattering, they lead to the production of more fragments. Furthermore, as illustrated in figure 10 the use of range shifters increases image noise in the simulated radiographs. Experimental investigation of the detection properties, especially when thick distal range shifters are used is necessary.

## V Conclusion

The residual helium range in mixed beam treatment plans was evaluated across several beam angles in lung cases, as well as in a prostate and a liver case, revealing that the helium range was too low in most scenarios. Three different strategies were applied to ensure sufficient helium range. The *EW He* strategy uses a mixed carbon-helium beam only for energies with sufficient helium range, otherwise a pure carbon beam is used. The *const RaShi* and *EW RaShi* incorporate proximal and distal range shifters to ensure sufficient helium range while also optimizing detection capabilities by incorporating the sensitive range of the detector in the selection of the range shifters.

Overall, all evaluated residual helium range strategies successfully ensure sufficient helium range. Strategies involving range shifters further increase the number of detectable spots. These strategies allow more flexibility in the chosen treatment angle. All of this increases the clinical usability of the mixed carbon-helium beam method, which shows promising potential for range verification, offering online beams-eye-view information, and allowing for the visualization of the treated patient's anatomy.

## Acknowledgments

This work was funded by the Deutsche Forschungsgemeinschaft (DFG, German Research Foundation) – Project No. 457509854.

## Conflict of interest

The authors declare that they have no known competing financial interests or personal relationships that could have appeared to influence the work reported in this paper.

---

\*<https://www.ptcog.site/index.php/facilities-in-operation-public>

## VI References

1. Mazzucconi D, Agosteo S, Ferrarini M, et al. Mixed particle beam for simultaneous treatment and online range verification in carbon ion therapy: Proof-of-concept study. *Medical Physics*. 2018;45(11). eprint: <https://onlinelibrary.wiley.com/doi/pdf/10.1002/mp.13219>:5234–5243.
2. Graeff C, Weber U, Schuy C, et al. [OA027] Helium as a range probe in carbon ion therapy. *Physica Medica*. Abstracts from the 2nd European Congress of Medical Physics.2018;52:11.
3. Graeff C, Volz L, Martire MC, et al. O072 / #772 - First experimental production of a mixed carbon/helium beam for online range monitoring and image guidance. *International Journal of Particle Therapy*. Proceedings to the 62nd Annual Conference of the Particle Therapy Cooperative Group (PTCOG).2024;12:100185.
4. Galonska M, Barth W, Graeff C, et al. First dual isotope beam production for simultaneous heavy ion radiotherapy and radiography. *JACoW*. 2024;IPAC2024:WEAN1.
5. Kausel M, Schmitzer C, Gsponer A, et al. A double multi-turn injection scheme for generating mixed helium and carbon ion beams at medical synchrotron facilities. arXiv:2501.12797 [physics]. 2025.
6. Renner E, Schmitzer C, Plassard F, et al. Towards the slow extraction of mixed He and C beams for online range verification. *JACoW*. 2024:THPR43.
7. Volz L, Kelleter L, Both S, et al. Experimental exploration of a mixed helium/carbon beam for online treatment monitoring in carbon ion beam therapy. *Physics in Medicine and Biology*. 2020;65(5). Publisher: IOP Publishing:055002.
8. Hardt JJ, Pryanichnikov AA, Homolka N, et al. The potential of mixed carbon-helium beams for online treatment verification: a simulation and treatment planning study. *Physics in Medicine and Biology*. 2024.
9. Wieser HP, Cisternas E, Wahl N, et al. Development of the open-source dose calculation and optimization toolkit matRad. *Medical Physics*. 2017;44(6). eprint: <https://onlinelibrary.wiley.com/doi/pdf/10.1002/mp.12251>:2556–2568.
10. Abbani N, Al-Hasnawi N, Ackermann B, et al. matRad. 2024.
11. Perl J, Shin J, Schumann J, Faddegon B, and Paganetti H. TOPAS: an innovative proton Monte Carlo platform for research and clinical applications. *Medical Physics*. 2012;39(11):6818–6837.
12. Faddegon B, Ramos-Méndez J, Schuemann J, et al. The TOPAS tool for particle simulation, a Monte Carlo simulation tool for physics, biology and clinical research. *Physica medica: PM: an international journal devoted to the applications of physics to medicine and biology: official journal of the Italian Association of Biomedical Physics (AIFB)*. 2020;72:114–121.
13. DeJongh EA, DeJongh DF, Polnyi I, et al. Technical Note: A fast and monolithic prototype clinical proton radiography system optimized for pencil beam scanning. *Medical physics*. 2021;48(3):1356–1364.

14. Pryanichnikov A, Hardt JJ, Martin L, et al. Experimental Single Plane Position Tracking Proton and Helium Pencil Beam Radiographs: Feasibility Study. *International Journal of Particle Therapy*. Proceedings to the 63rd Annual Conference of the Particle Therapy Cooperative Group (PTCOG).2025.
15. Pryanichnikov AA, Hardt JJ, DeJongh EA, et al. Feasibility study of using fast low-dose pencil beam proton and helium radiographs for intrafractional motion management. *Physica Medica: European Journal of Medical Physics*. 2025;133. Publisher: Elsevier.
16. Krah N, Khellaf F, Létang JM, Rit S, and Rinaldi I. A comprehensive theoretical comparison of proton imaging set-ups in terms of spatial resolution. *Physics in Medicine & Biology*. 2018;63(13):135013.
17. Ordoñez CE, Karonis NT, Duffin KL, et al. Fast in situ image reconstruction for proton radiography. *Journal of Radiation Oncology*. 2019;8(2):185–198.
18. Siddon RL. Fast calculation of the exact radiological path for a three-dimensional CT array. *Medical Physics*. 1985;12(2):252–255.
19. Wang M, Zhang L, Zheng J, Li G, Dai W, and Dong L. Investigating the effects of a range shifter on skin dose in proton therapy. *Nuclear Engineering and Technology*. 2023;55(1):215–221.
20. Tripathi RK, Cucinotta FA, and Wilson JW. Accurate universal parameterization of absorption cross sections III – light systems. *Nuclear Instruments and Methods in Physics Research Section B: Beam Interactions with Materials and Atoms*. 1999;155(4):349–356.
21. Horst F, Aricò G, Brinkmann KT, et al. Measurement of He 4 charge- and mass-changing cross sections on H, C, O, and Si targets in the energy range 70–220 MeV/u for radiation transport calculations in ion-beam therapy. *Physical Review C*. 2019;99(1):014603.
22. Hong L, Goitein M, Bucciolini M, et al. A pencil beam algorithm for proton dose calculations. *Physics in Medicine & Biology*. 1996;41(8). Publisher: IOP Publishing:1305.
23. Hugo GD, Weiss E, Sleeman WC, et al. Data from 4D Lung Imaging of NSCLC Patients (Version 2) [Data set]. 2016.
24. Craft D, Bangert M, Long T, Papp D, and Unkelbach J. Shared data for intensity modulated radiation therapy (IMRT) optimization research: the CORT dataset. *Giga-Science*. 2014;3(1):2047–217X–3–37.
25. Gehrke T, Gallas R, Jäkel O, and Martišíková M. Proof of principle of helium-beam radiography using silicon pixel detectors for energy deposition measurement, identification, and tracking of single ions. *Medical Physics*. 2018;45(2):817–829.
26. Metzner M, Zhevachevska D, Schlechter A, et al. Energy painting: helium-beam radiography with thin detectors and multiple beam energies. *Physics in Medicine and Biology*. 2024;69(5).
27. Krah N, Dauvergne D, Létang JM, Rit S, and Testa É. Relative stopping power resolution in time-of-flight proton CT. *Physics in Medicine & Biology*. 2022;67(16). Publisher: IOP Publishing:165004.

28. Ulrich-Pur F, Bergauer T, Galatyuk T, et al. First experimental time-of-flight-based proton radiography using low gain avalanche diodes. *Physics in Medicine & Biology*. 2024;69(7). Publisher: IOP Publishing:075031.
29. Volz L, Korte J, Martire MC, et al. Opportunities and challenges of upright patient positioning in radiotherapy. *Physics in Medicine & Biology*. 2024;69(18). Publisher: IOP Publishing:18TR02.